NANO LETTERS

Letter

pubs.acs.org/NanoLett

Density-Gradient-Free Microfluidic Centrifugation for Analytical and Preparative Separation of Nanoparticles

Paolo Arosio,[†] Thomas Müller,[†] L. Mahadevan,[‡,§] and Tuomas P. J. Knowles*[,†]

[†]Department of Chemistry, University of Cambridge, Lensfield Road, Cambridge CB2 1EW, United Kingdom

[‡]School of Engineering and Applied Sciences, Harvard University, 29 Oxford Street, Cambridge, Massachusetts 02138, United States

[§]Department of Physics, Harvard University, 17 Oxford Street, Cambridge, Massachusetts 02138, United States

Supporting Information

ABSTRACT: Sedimentation and centrifugation techniques are widely applied for the separation of biomolecules and colloids but require the presence of controlled density gradients for stable operation. Here we present an approach for separating nanoparticles in free solution without gradients. We use microfluidics to generate a convective flow perpendicular to the sedimentation direction. We show that the hydrodynamic Rayleigh−Taylor-like instability, which, in traditional methods, requires the presence of a density gradient, can be suppressed by the Poiseuille flow in the microchannel. We illustrate the power of this approach by demonstrating the separation of mixtures of particles on the nanometer scale, orders of magnitude smaller than the micrometer-sized objects separated by conventional inertial microfluidic approaches. This technique exhibits a series of favorable features including short analysis time, small sample volume, limited dilution of the analyte, limited interactions with surfaces as well as the possibility to tune easily the separation range by adjusting the geometry of the system. These features highlight the potential of gradient-free microfluidic centrifugation as an attractive route toward a broad range of nanoscale applications.

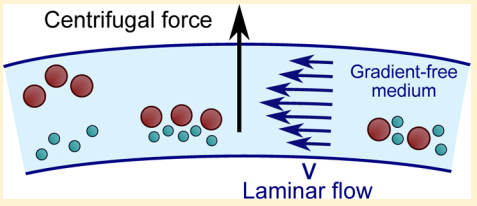

KEYWORDS: *Centrifugal separation, microfluidic, colloids, nanoparticles, density gradient, hydrodynamic instability*

Separation of colloids and biomolecules for both analytical and preparative purposes is a central element of many areas of nanoscience and technology. Among various available fractionation methods, such as chromatography, field-flow fractionation, and electrophoresis,[1] analytical ultracentrifugation techniques provide high resolution at the nanometer scale and are widely applied in biochemistry and biophysics to separate cellular components and macromolecular complexes.[2−5] These powerful and versatile technologies rely on the differential force induced by a gravitational or centrifugal field on objects with different masses and provide relevant information on the size and shape of nanoparticles and macromolecular complexes.[6−8]

In principle, sedimentation techniques may be used for preparative purposes simply by layering a sample of the mixture on top of a liquid volume and letting the different components sediment under the inertial field. However, due to a fluid dynamic Rayleigh−Taylor-like instability, the analyte would sink in the underlying liquid behaving as a single complex fluid rather than a dispersion of individual particles.[9−11] To avoid this instability problem in sedimentation and band ultracentrifugation techniques, the underlying liquid requires the presence of a density gradient which is obtained by addition of inert molecules, typically heavy salts or sugars.[12,13]

Despite being the traditional method for preparative centrifugation in biology and biochemistry, the presence of the gradients poses challenges regarding their preparation and stability during separation.

Moreover, interactions between the analyte and the molecules of the density gradient act in addition to the gravitational and buoyancy forces; as a consequence, the position of the separating molecules in the gradient can depend on the chemical nature of the molecules used to create the gradient and is difficult to be predicted a priori.[14]

To address this challenge, in this work we describe an approach based on inertial microfluidics. This strategy allows the separation of particles in the presence of convective flow which removes the hydrodynamic instability and therefore the need of the density gradient. The technique has analogies with sedimentation field-flow fractionation (FFF)[15−17] but operates without the requirement for surface interactions and is implemented with microfluidic technology, a factor which offers a series of advantages such as high throughput, low cost, control of stable laminar flow profiles, limited interactions with surfaces, and small volume of the separation units.[18−20] Furthermore, the fractionated samples are not diluted significantly during the separation and can be concentrated in collectors located at the end of the separation cell, thus facilitating recovery of the material and subsequent analysis.

Received: December 23, 2013
Revised: March 3, 2014
Published: March 10, 2014

In the last years centrifugal microfluidic devices have been developed for the separation of objects at the micrometer scale, with particular attention to cells and blood components.[21−24]

By contrast, achieving separation in the colloidal nanometer range has proven challenging due to the degradation of the separative power induced by the increased propensity of nanoparticles to diffuse. One of the few successful examples is represented by centrifugal SPLITT fractionation, which has been applied to the fractionation of submicrometer particles on a large scale.[12] However, it remains a challenge to develop devices capable of separating objects at the nanometer scale from both an analytical and a preparative point of view. Herein, we show that by tuning the geometry and in particular the retention time in the separation channel of our device it is possible to extend significantly the separation range of centrifugal microfluidic techniques and obtain fractionation resolution in the nanometer range.

The separation occurs in a characteristic time of a few minutes, substantially shorter than the time required typically by traditional centrifugal analysis on bulk scales. This short analysis time could open the possibility for the study of the stoichiometry and kinetics of transient complexes, currently not achievable with conventional techniques.

In addition, the separation is not affected by liquid composition, allowing the analysis and the fractionation of particles and molecules in their native environment without requiring sample preparation which can potentially perturb the original configuration. The microfluidic technique described here forms the basis for a *lab-on-a-chip* platform which can be implemented using standard soft lithography and is applicable to a broad range of systems from biological, environmental, and physical sciences to nanotechnology.

Microfluidic Centrifugation under Flow. We perform the separation of a flowing particle dispersion by applying a centrifugal force field perpendicularly to the axis of flow. This geometry is similar to sedimentation field-flow fractionation, but interactions of the analytes with a surface are not required. Convective flow in the presence of a centrifugal field can be induced by designing a device with the inlet and the outlet located at different distances from the center of rotation resulting in a net hydrostatic pressure difference.

We implemented this concept in a microfluidic device fabricated with standard soft lithography methods.[25] A picture of the device is shown in Figure 1a, and the principle of the technique is illustrated in Figure 1b and c.

In the presence of a centrifugal field, the pressure difference at the inner inlets (r_1) and the outer outlet (r_2) generates a convective velocity v inside the separation channel equal to

$$v = \frac{1}{2}\rho_f \omega^2 (r_2^2 - r_1^2)\frac{1}{R_{Tot}}\frac{1}{A} \quad (1)$$

where R_{Tot} is the total hydrodynamic resistance of the device, A is the cross sectional area of the channel, ω is the rotational angular velocity, and ρ_f is the density of the fluid.

The separation occurs inside a channel of rectangular cross section where low Reynolds number flow occurs in the laminar regime. At the beginning of the channel, the beam of the particle dispersion is focused between two layers of an auxiliary liquid which is introduced in a separate inlet aligned along the radial distance with the analyte inlet (Figure 1b). The analyte and the auxiliary fluid are loaded into the designated inlet reservoirs prior to centrifugation by means of elastic tubing and syringe.

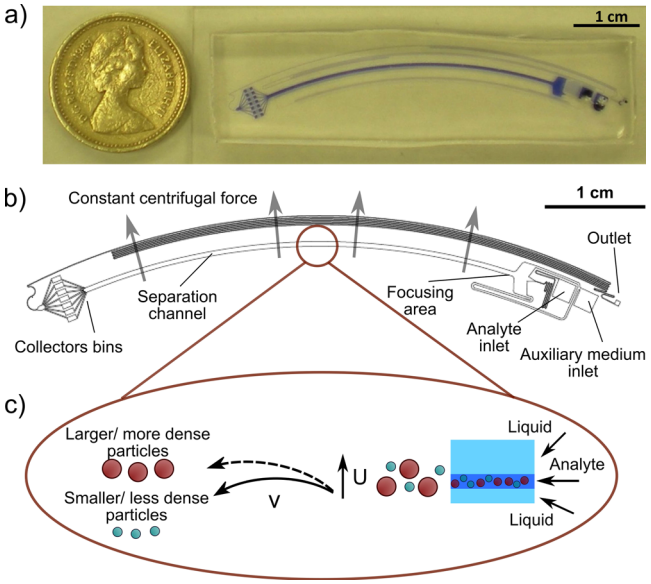

Figure 1. Description of the microfluidic centrifugal device. a) Picture of the microfluidic device, where the channels have been filled with a Commassie blue solution for visualization; b) scheme of the device and most relevant components; c) principle of the separation mechanism in the channel.

While flowing along the separation channel the analyte beam is subjected to a centrifugal force acting perpendicularly to the axis of flow. This force is balanced by the hydrodynamic drag force and by the buoyancy force, resulting in a steady state velocity, u, given by

$$u = \frac{(\rho_p - \rho_f)}{18\mu} D_p^2 r_d \omega^2 = s r_d \omega^2 \quad (2)$$

where D_p is the particle diameter, ρ_p the particle density, r_d the distance from the center of rotation, μ the fluid viscosity, and s the sedimentation coefficient.

From eq 2 it can be seen that the migration velocity u and therefore the migration distance are proportional to the square of the particle size and to the particle density. Larger and denser particles will move away from the center of rotation, while smaller and less dense particles will be less deflected (Figure 1c).

The position of the analyte beam in the channel has been designed to exhibit an asymmetry with respect to the center of the channel in order to increase the width available for separation. Specifically, the center of the analyte beam is located 380 μm away from the farther wall of the separation channel which has a width of 500 μm. The width of the analyte beam can be readily tuned by changing the resistances of the analyte and of the auxiliary buffer solution. A narrow analyte beam is beneficial for the separation resolution.

At the end of the separation channel, a flow splitter collects the fractionated particles in different bins, as shown in Figure 1b. The accumulated material can be recovered from the bins after the separation, for example by extraction through the polydimethylsiloxane (PDMS) layer, allowing further analysis of the fractionated samples. As a consequence, the proposed device can be used not only for analytical but also for preparative purposes. The number and size of the bins can be easily adjusted to optimize specific requirements.

dx.doi.org/10.1021/nl404771g | Nano Lett. 2014, 14, 2365−2371

From the basic principles of the technique we can calculate the relevant parameters for the separation.

The resolution of the fractionation is strongly dependent on the retention time of the particles in the channel, $\tau = L_C/v$, with L_C the length of the separation channel. If the centrifugal force is applied for a time longer than the retention time, as is the case under steady-state operation, the migration distance traveled by the particles is equal to $L_u = u\tau$. Equations 1 and 2 indicate the parameters of the systems which can be modified to tune the separation resolution. In particular, the separation of small objects requires a large retention time in the channel, and therefore a small convective flow, which according to eq 1 can be achieved by decreasing the relative distance between inlet and outlet, $r_2^2 - r_1^2$, by increasing the total resistance of the device R_{Tot} and/or by increasing the cross section A of the separation channel.

In addition, since the distance due to diffusion depends on the square root of the time $L_{Diff} = (2D\tau)^{1/2}$ while the migration distance is linearly proportional to the time $L = u\tau$, large residence times favor the relative contribution of centrifugal migration over diffusion on the particle motion.

The microfluidic device was centrifuged on a custom-made mechanical rotor described in the scheme in Figure 2. The microscope glass slides forming the bottom part of our microfluidic devices fit into the cavities of a thin aluminum disk which is sandwiched between two thick Perspex disks.

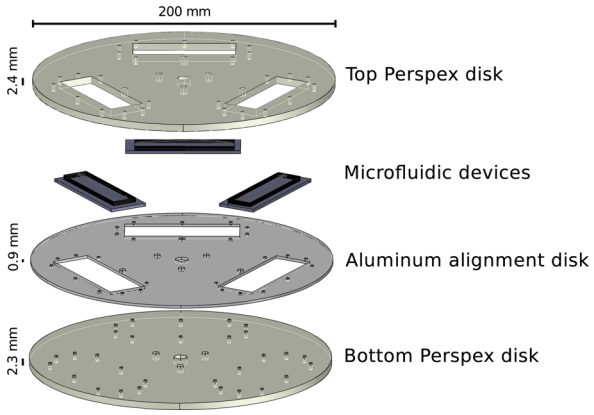

Figure 2. Schematic of the rotor design. The microscope glass slides forming the bottom part of the microfluidic devices fit into the 76 × 26 mm cavities of a 0.9 mm thick aluminum disk which is sandwiched between two roughly 2.3 mm thick Perspex disks. The 68 × 24 mm rectangular holes in the top disk are smaller than the glass slides to keep them in place but allow the PDMS part of the devices to protrude. The distance between the center of rotation and the center of the glass slides is 63 mm.

Separation of Nanoparticles. We separate aqueous dispersions of fluorochrome-functionalized polystyrene nanoparticles with nominal diameters of 50, 100, and 200 nm and a density of 1.06 kg/m^3 at a volume fraction of about 0.05%. Milli-Q distilled water was used as auxiliary fluid.

Initially, the channels of the device were filled with the auxiliary medium and the analyte solution by an external pump. In Figure 3 we show the position of the particles before centrifugation by bright field and fluorescent illumination of selected relevant areas of the microfluidic device.

Before applying the technique to the separation of mixtures, we verify the capability of the device to deflect a beam of monodisperse dispersions of the particles.

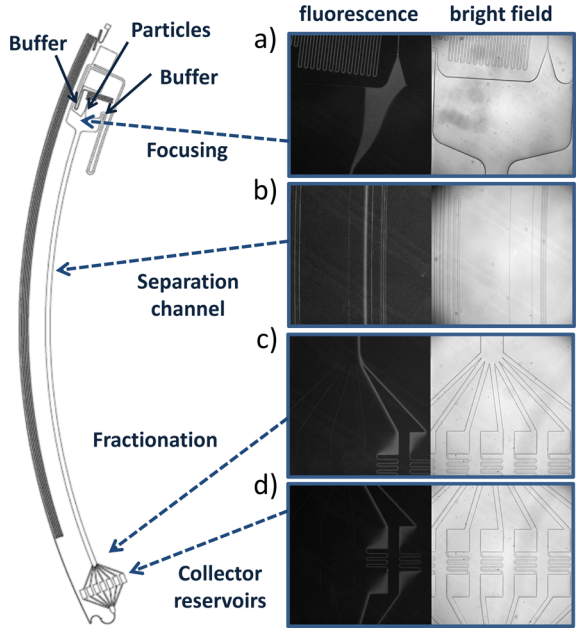

Figure 3. Initial position of the particle beam in the absence of inertial field. The analyte solution is focused in the separation channel in a narrow beam between two layers of an auxiliary medium, a). The beam crosses the channel, where, in the presence of a centrifugal force, separation will occur in a direction perpendicular to the flow, b). At the end of the channel the fractionated particles are collected in different bins, c–d).

The particle position in the bins before and after centrifugation of the device at 5000 rpm for 5 min is shown in the fluorescence pictures and in the histograms in Figure 4, which report the normalized fluorescence intensities integrated in the different bins. The error bars represent the standard deviation of at least three repetitions. The data show that bigger particles are progressively shifted toward the outer part of the separation channel. To quantify the migration distances induced by centrifugation, we fitted the histograms with a Gaussian distribution, and we considered the mean values as average migration distances. We applied in a first instance the Gaussian distribution, which represents the probability distribution of particles diffusing laterally under a block flow starting from a narrow initial distribution, although the flow is Poiseuille and the migration induced by centrifugation overimposes the diffusion motion. As a consequence, we do not expect the Gaussian distribution to describe accurately the distribution of the particles in the bins, and it has been rather employed here as a help to quantify the migration distances. We applied this procedure to the conditions where the analyte is not deflected too close to the wall. The measured migration distances, summarized in Table 1, are 28 ± 19 μm for the 50 nm and 144 ± 47 μm for the 100 nm particles, while the 200 nm particles are pushed toward the outer wall of the channel, indicating a migration distance larger than 380 μm. Remarkably, these values are in good agreement with the migration distances predicted by eq 2 (see Table 1 and SI). This confirms the robustness of our fractionation technique and allows the design of separation based on a first-principles approach without the need of any calibration, provided that information about the sedimentation coefficient (i.e., size, shape, and density) of the analytes are known.

dx.doi.org/10.1021/nl404771g | Nano Lett. 2014, 14, 2365–2371

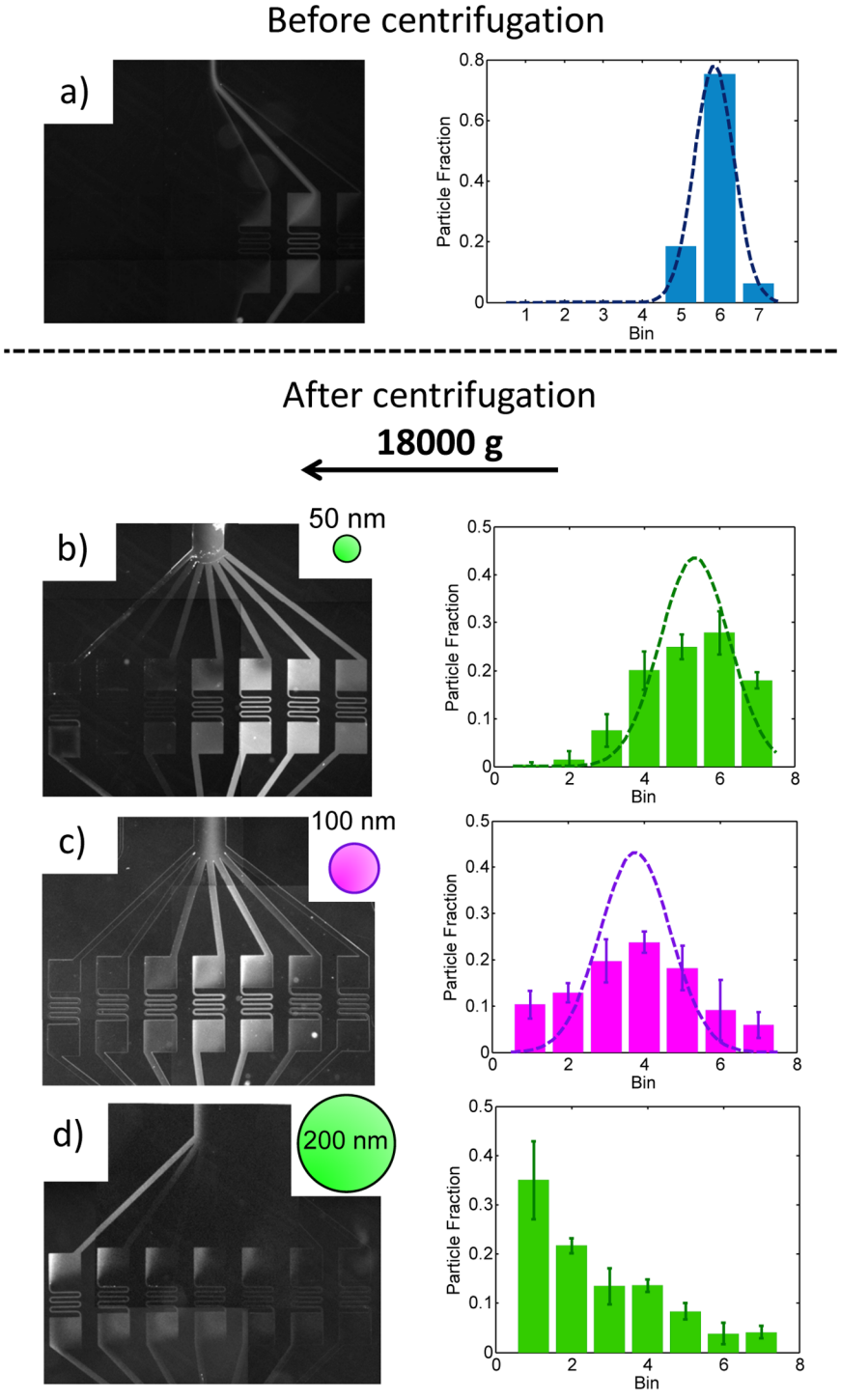

Figure 4. Separation of nanosized colloids by microfluidic centrifugation. Position of monodisperse particle dispersions in the collector bins before a) and after b)−d) centrifugation. Particle sizes are 50 nm (green) b), 100 nm (red) c), and 200 nm (green) d).

Alternatively, for particles with unknown parameters the calibration of the device allows the estimation of the mass of the particles by measurements of the migration distances.

After applying the device to monodisperse particle dispersions, we demonstrate the separation power of the technique by fractionating a latex mixture of red-fluorescent 100 nm colloids and green-fluorescent 200 nm colloids. Microspheres with different fluorescence properties have been used in order to allow the identification of the position of the different particles before and after the separation. In Figure 5 it can be seen that before centrifugation the fluorescent signals of the two different particle populations overlap in a single beam, indicating the presence of a homogeneous mixture. After centrifugation, the 200 nm particles are deflected more than 380 μm and pushed toward the edge of the separation channel, while the beam of 100 nm particles migrates 152 ± 26 μm, indicating successful separation of the two populations. The migration of the particles in the mixture is very similar to the behavior of the single monodisperse particle dispersions shown

dx.doi.org/10.1021/nl404771g | *Nano Lett.* 2014, 14, 2365−2371

Table 1. Comparison between the Migration Distances Measured Experimentally in Figure 4 and the Migration Distances Predicted by Equation 2[a]

particle diameter	migration distance measured experimentally (μm)	migration distance calculated according to eq 2 (μm)	particle motion due to diffusion (μm) ($(2D\tau)^{1/2}$)
50 nm	28 ± 19	24.5	58
100 nm	144 ± 47	98	41
200 nm	>380	393	29

[a]Distances traveled by diffusive motion are also reported.

in Figure 5, indicating negligible interactions between the particles during separation.

We note that the selectivity of the separation can be optimized by modifying the parameters discussed in this work. For instance, the separation resolution could be improved by a narrower analyte beam or by increasing the length of the channel and the number of collector reservoirs. In addition, the current approach could be implemented in combination with a second separation technique to remove possible degeneracies with complex mixtures where particles with the same sedimentation coefficient can be present.

Presence of Laminar Flow Removes the Hydrodynamic Instability. The operation of centrifugal separation techniques in bulk is limited by a Rayleigh−Taylor instability, which is commonly observed when a denser liquid is placed on top of a lighter liquid and originates from irregularities occurring at the interface between the two liquids.[10,11] Rayleigh−Taylor-like instabilities are also observed with colloidal dispersions with no surface tension. In these systems, particle velocities become correlated and propagate nascent density fluctuations at a velocity lager than the Stokes flow.[11] If the wavelength of the oscillations is smaller than a critical value, the Brownian motion of the particles counteracts the fluctuations, and the system remains stable.[9,11,26,27] On the contrary, if the fluctuations are sufficiently large, they induce portions of the heavier liquid to sink and portions of the lighter liquid to rise, developing fingers and eventually leading the whole particle dispersion to sink.

The relevant dimensionless parameter defining this behavior is the Rayleigh number[28]

$$\mathcal{R} = \frac{WK\Delta\rho g}{\mu D} \tag{3}$$

where $K = H^2/12$ is the effective permeability of the channel, H and W are the height and the width of the channel, respectively, $\Delta\rho$ is the excess density of the particle dispersion over pure water (equal to about 2.5×10^{-4} kg/m^3 for a dispersion containing 0.05% polystyrene particles), μ is the water viscosity, D is the particle diffusivity, and $g = r\omega^2$ is the centrifugal force in the channel.

In our system, the large value of $\mathcal{R} = 1300$ indicates that diffusion alone cannot counteract the propagation of the fingers and that instability would occur in the absence of flow. On the other hand, the experiments shown in the previous section clearly indicate that separation of nanoparticles in a mixture can be achieved in the presence of laminar Poiseuille flow even in the absence of density gradient and no hydrodynamic instability occurs. Indeed, the position of the beam at the inlet of the

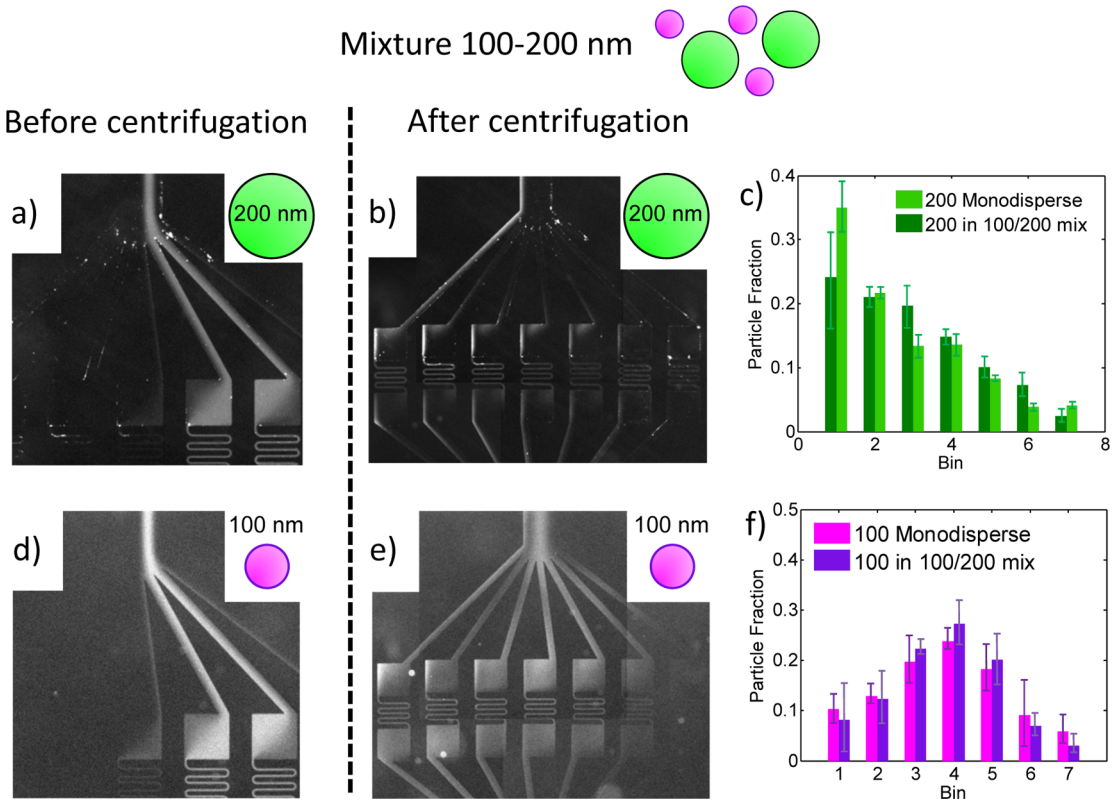

Figure 5. Separation of mixture of nanoparticles by microfluidic centrifugation. Position of the particles at the end of the separation channel and in the collector bins before a),b) and after d),e) centrifugation. Green-fluorescent 200 nm particles are visualized in a) and b), and red-fluorescent 100 nm particles are shown in d and e. c),f) The deflection of the particles in the mixture and in the monodisperse dispersions are compared.

dx.doi.org/10.1021/nl404771g | Nano Lett. 2014, 14, 2365−2371

separation channel before and after centrifugation is unaffected, as shown in Figure 6a, despite the application of a centrifugal force equal to 18000 *g*. The same particle dispersion is not, however, stable even at 1 *g* in the absence of the flow (Figure 6b). Under the gravitational force of 1 *g* the droplets sink in few seconds in the underlying water behaving as a single complex fluid. The same behavior is observed when a similar experiment is repeated in a microfluidic device under centrifugal field in the absence of flow (data not shown).

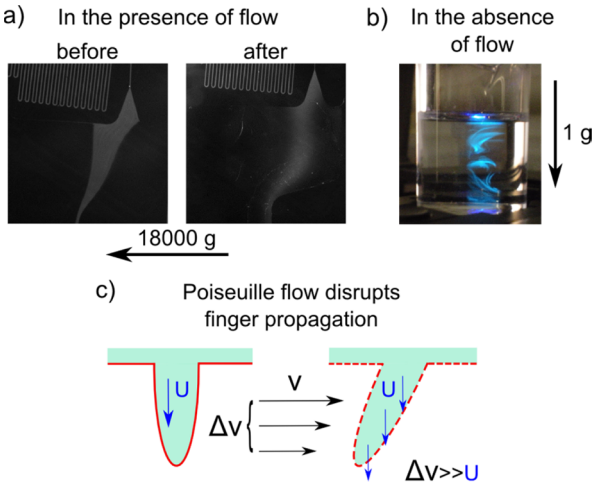

Figure 6. Removal of hydrodynamic instability in the presence of convective Poiseuille flow. a) Fluorescent images of the inlet of the separation channel before and after 5 min centrifugation at 5000 rpm, corresponding to 18000 *g*. The position of the beam is unaffected. b) In the absence of convective flow, droplets of the particle dispersion at the same volume fraction as in panel a sink in few seconds in the underlying liquid even under 1 *g*. c) Scheme of the removal of the hydrodynamic instability by the presence of the laminar Poiseuille flow. The rate of disruption of the fingers due to the relative movement of particles located at different positions along the height of the channel is faster than the rate of propagation of the fingers along the width of the channel.

This behavior is explained by considering the gradient of the flow velocity inside the channel, which is able to disrupt the development of the fingers by shifting different layers of particles located at different positions along the height of the channel (Figure 6c). Indeed, a simple scaling analysis shows that the velocity gradient of the Poiseuille flow $\nabla V \approx 5 \times 10^{-4}$ m/s is 1 order of magnitude larger than the advection velocity of the fingers in the underlying liquid: $U = K\Delta\rho g/\mu \approx 2 \times 10^{-5}$ m/s. Therefore, the rate of disruption of the fingers due to the relative movement of the particles is faster than the rate of propagation of the fingers along the height of the channel. We can formalize this scaling analysis by defining an analog of the dimensionless Rayleigh number in the presence of convective flow in the laminar regime

$$\mathcal{R}_V = \frac{K\Delta\rho g}{\mu\nabla V} \tag{4}$$

where the diffusion term is replaced by the gradient of the velocity. The instability is absent at low $\mathcal{R}_V$ values and present at large $\mathcal{R}_V$ values. In our system, $\mathcal{R}_V \approx 0.04$.

It is worth noting that the presence of the velocity gradient, rather than the generic presence of flow, plays a key role in the disruption of the fingers and that instability is expected to occur in the presence of plug flow.

In addition, we note that the characteristic time scale of diffusion of the nanoparticles along the height of the channel ($\tau_{Diff} = (H/2)^2/(2D) \approx 35$ s) is smaller than the time scale of the separation ($\tau = L_C/v \approx 200$ s). The corresponding Peclet number (Pe) is equal to $Pe = \tau_{Diff}/\tau_{Conv} \approx 0.175$. As a consequence, during the residence time in the separation channel the particles sample the entire vertical velocity distribution due to their diffusive motion, and therefore the effect of the parabolic velocity profile along the height of the channel can be neglected for the separation.

Conclusions. We have designed an approach to eliminate hydrodynamic instabilities in centrifugation to allow for stable operation even in the absence of density gradients required by conventional methods. We demonstrate the power of this approach by separating nanoparticle dispersions in the presence of a flow occurring perpendicularly to the separation direction. By tuning the device geometry and therefore the retention time in the separation channel we achieved separation of particles in the nanometer size range, orders of magnitude smaller than the micrometer-sized objects separated by current microfluidic devices. The migration distances measured experimentally are in excellent agreement with theoretical predictions, confirming the robustness of the technique.

The device exhibits highly advantageous features such as limited dilution of the sample as well as the limited interactions with surfaces. In addition, the separation occurs in a characteristic time of a few minutes, significantly shorter than the analysis time required by current centrifugal techniques.

■ ASSOCIATED CONTENT

Ⓢ Supporting Information

Material and methods, calculation of the migration distances, and considerations on the accumulation of particles on the wall of the reservoir during centrifugation (Figure S1). This material is available free of charge via the Internet at http://pubs.acs.org.

■ AUTHOR INFORMATION

Corresponding Author

*E-mail: tpjk2@cam.ac.uk.

Author Contributions

P.A., T.M., and T.P.J.K. designed the study. P.A. and T.M. performed the experiments. P.A., T.M., L.M., and T.P.J.K. analyzed the data. P.A., T.M., and T.P.J.K. wrote the paper. All authors discussed the results and commented on the manuscript.

Notes

The authors declare no competing financial interest.

■ ACKNOWLEDGMENTS

We thank the Swiss National Science Foundation (P.A., T.M.), the BBSRC (T.P.J.K., T.M.) and the Newman Foundation (TPJK) for financial support. We are grateful to Simon Dowe and the mechanical workshop at the Department of Chemistry of the University of Cambridge for their help with designing and fabricating the centrifuge rotor disks.

■ REFERENCES

(1) Fedotov, P. S.; Vanifatova, N. G.; Shkinev, V. M.; Spivakov, B. Y. *Anal. Bioanal. Chem.* **2011**, *400* (6), 1787−1804.

(2) Chou, C. Y.; Jen, W. P.; Hsieh, Y. H.; Shiao, M. S.; Chang, G. G. *J. Biol. Chem.* **2006**, *281* (19), 13333−13344.
(3) Howlett, G. J.; Minton, A. P.; Rivas, G. *Curr. Opin. Chem. Biol.* **2006**, *10* (5), 430−436.
(4) Lebowitz, J.; Lewis, M. S.; Schuck, P. *Protein Sci.* **2002**, *11* (9), 2067−2079.
(5) Rivas, G.; Stafford, W.; Minton, A. P. *Methods* **1999**, *19* (2), 194−212.
(6) Cole, J. L.; Lary, J. W.; Moody, T. P.; Laue, T. M. Analytical ultracentrifugation: Sedimentation velocity and sedimentation equilibrium. In *Biophysical Tools for Biologists*, Vol. 1 in Vitro Techniques; Correia, J. J., Detrich, H. W., Eds.; 2008; Vol. *84*, pp 143−179.
(7) Schuck, P. *Biophys. J.* **2000**, *78* (3), 1606−1619.
(8) Schuck, P.; Perugini, M. A.; Gonzales, N. R.; Howlett, G. J.; Schubert, D. *Biophys. J.* **2002**, *82* (2), 1096−1111.
(9) Jerri, H. A.; Sheehan, W. P.; Snyder, C. E.; Velegol, D. *Langmuir* **2010**, *26* (7), 4725−4731.
(10) Sharp, D. H. *Physica D* **1984**, *12* (1−3), 3−18.
(11) Wysocki, A.; Royall, C. P.; Winkler, R. G.; Gompper, G.; Tanaka, H.; van Blaaderen, A.; Loewen, H. *Soft Matter* **2009**, *5* (7), 1340−1344.
(12) Fuh, C. B.; Myers, M. N.; Giddings, J. C. *Ind. Eng. Chem. Res.* **1994**, *33* (2), 355−362.
(13) Martin, R. G.; Ames, B. N. *J. Biol. Chem.* **1961**, *236* (5), 1372−1379.
(14) Piazza, R.; Buzzaccaro, S.; Secchi, E.; Parola, A. *Soft Matter* **2012**, *8* (27), 7112−7115.
(15) Giddings, J. C. *Science* **1993**, *260* (5113), 1456−1465.
(16) Li, J. M.; Caldwell, K. D.; Machtle, W. *J. Chromatogr.* **1990**, *517*, 361−376.
(17) Williams, S. K. R.; Raner, G. M.; Ellis, W. R.; Giddings, J. C. *J. Microcolumn Sep.* **1997**, *9* (3), 233−239.
(18) Cho, S.; Kang, D.-K.; Choo, J.; deMello, A. J.; Chang, S.-I. *BMB Rep.* **2011**, *44* (11), 705−712.
(19) Ducree, J.; Haeberle, S.; Lutz, S.; Pausch, S.; von Stetten, F.; Zengerle, R. *J. Micromech. Microeng.* **2007**, *17* (7), S103−S115.
(20) Gorkin, R.; Park, J.; Siegrist, J.; Amasia, M.; Lee, B. S.; Park, J.-M.; Kim, J.; Kim, H.; Madou, M.; Cho, Y.-K. *Lab Chip* **2010**, *10* (14), 1758−1773.
(21) Burger, R.; Kirby, D.; Glynn, M.; Nwankire, C.; O'Sullivan, M.; Siegrist, J.; Kinahan, D.; Aguirre, G.; Kijanka, G.; Gorkin, R. A., III; Ducree, J. *Curr. Opin. Chem. Biol.* **2012**, *16* (3−4), 409−414.
(22) Cho, Y.-K.; Lee, J.-G.; Park, J.-M.; Lee, B.-S.; Lee, Y.; Ko, C. *Lab Chip* **2007**, *7* (5), 565−573.
(23) Haeberle, S.; Brenner, T.; Zengerle, R.; Ducree, J. *Lab Chip* **2006**, *6* (6), 776−781.
(24) Morijiri, T.; Sunahiro, S.; Senaha, M.; Yamada, M.; Seki, M. *Microfluid. Nanofluid.* **2011**, *11* (1), 105−110.
(25) Siegel, A. C.; Bruzewicz, D. A.; Weibel, D. B.; Whitesides, G. M. *Adv. Mater.* **2007**, *19* (5), 727−733.
(26) Loewen, H. *Soft Matter* **2010**, *6* (14), 3133−3142.
(27) Velegol, D.; Shori, S.; Snyder, C. E. *Ind. Eng. Chem. Res.* **2009**, *48* (5), 2414−2421.
(28) Slim, A. C.; Bandi, M. M.; Miller, J. C.; Mahadevan, L. *Phys. Fluids* **2013**, *25* (2), 024101−1/20.